RESEARCH ARTICLE | APRIL 23 2025

First-principles study of the structural, electronic, mechanical, and optical properties of Zintl-phase K_2AgBi ternary compound for optoelectronic applications

John Peter Kachira; Robinson Musembi ; Francis Nyongesa; Mwende Mbilo ; Martin Nyamuga ; Ibrahim Musanyi

AIP Advances 15, 045126 (2025)
https://doi.org/10.1063/5.0267495

First-principles study of the structural, electronic, mechanical, and optical properties of Zintl-phase K_2AgBi ternary compound for optoelectronic applications

Cite as: AIP Advances 15, 045126 (2025); doi: 10.1063/5.0267495
Submitted: 24 February 2025 • Accepted: 10 April 2025 •
Published Online: 23 April 2025

John Peter Kachira,[1,2] Robinson Musembi,[1,a)] Francis Nyongesa,[1] Mwende Mbilo,[1] Martin Nyamuga,[1] and Ibrahim Musanyi[1]

AFFILIATIONS

[1] Monolith Research Group, Department of Physics, Faculty of Science and Technology, University of Nairobi, P.O. Box 30197, 00100 Nairobi, Kenya
[2] Department of Natural Sciences, Mbeya University of Science and Technology, P.O. Box 131, Mbeya, Tanzania

[a)] **Author to whom correspondence should be addressed:** musembirj@uonbi.ac.ke

ABSTRACT

A comprehensive first-principles study was conducted to explore the structural, electronic, mechanical, thermophysical, and optical properties of a Zintl-phase K_2AgBi ternary semiconductor compound using density functional theory. The calculations employed the local density approximation (LDA), generalized gradient approximation (GGA), and meta-GGA methods. The computed negative formation energies proved the thermodynamic stability of the K_2AgBi ternary compound. The computed bandgap values were 0.6732 and 0.7848 eV for the LDA and GGA, respectively. More refined bandgap estimates were obtained using meta-GGA methods, with the Tran–Blaha modified Becke–Johnson potential yielding 0.9346 eV and the revised strongly constrained and appropriately normed functional yielding 0.9778 eV. The projected density of states study revealed that the Ag3d, Bi2p, and K1s orbitals dominate the formation of the valence band, whereas the K4p, Ag2p, and K2s orbitals contribute significantly to the formation of the conduction band. Analysis of the mechanical properties confirmed that K_2AgBi is mechanically stable and ductile. Optical analysis revealed strong absorption in the 1.0–15 eV energy range, high refractive index in the low-energy region, and distinct plasmonic response, suggesting potential applications in photovoltaics, optoelectronics, and plasmonic-based technologies.

I. INTRODUCTION

The semiconductor industry plays a fundamental role in modern technological advancements, particularly in optoelectronic and photovoltaic (PV) applications.[1] These materials are essential for developing energy-efficient and sustainable devices for use in telecommunications, consumer electronics, medical diagnostics, defense, and renewable energy systems.[2] Among the semiconductor technologies, photovoltaic devices have gained prominence as a workable response for green energy production.[1,3] However, the widespread use of silicon solar cells, which dominate the current photovoltaic market, has significant limitations.[4] The cost-intensive fabrication processes, low absorption coefficient near the bandgap, and inherent brittleness of silicon restrict its efficiency and applicability, particularly in flexible and next-generation solar technologies. Such limitations have driven research toward alternative materials that are both cost-effective and environmentally sustainable while maintaining high efficiency.[2,5]

The pursuit of novel semiconducting materials has been central to advancing optoelectronic and photovoltaic technologies. Among the emerging material families, Zintl-phase pnictide ternary semiconductors have gained attention due to their tunable electronic

properties, structural diversity, and potential for eco-friendly composition.[3,6] Some pnictide materials exist in a Zintl phased structure derived from the concept proposed by Eduard Zintl in the 1930s. These compounds are formed from the combination of elements from the electropositive group I_A (K, Na, Cs, and Rb) or group II_A (Sr, Mg, Ca, and Ba) with group V_A (As, P, Sb, and Bi) and group I_B (Cu, Au, and Ag).[3,7] Zintl-phase compounds exhibit unique bonding environments that balance ionic and covalent interactions.[8] Unlike silicon, many Zintl-phase materials feature high Seebeck coefficients, low thermal conductivities, and versatile electronic structures, making them ideal for applications in photovoltaics, thermoelectrics, and optoelectronics.[9] Recent studies highlight the versatility of these compounds in delivering desirable optoelectronic characteristics. For instance, Zintl phases such as Ba_2As_5 and related arsenides show promising bandgaps and absorption properties suitable for photovoltaic integration. In addition, computational investigations suggest that their band structures can be engineered to optimize light absorption and carrier transport, critical for solar energy conversion and photodetector design. Moreover, their composition often relies on earth-abundant and non-toxic elements, aligning with the global push for sustainable and environmentally friendly technologies.[10,11]

Few studies on Zintl-phase compounds similar to those studied have been reported in the literature. Musembi and Mbilo studied the structural, electronic, elastic, mechanical, and optical properties of K_2AgAs Zintl-phase ternary semiconductor compounds using the first-principles method.[12] This investigation showed that K_2AgAs can be synthesized and applied as active photoactive materials in solar cells. In another study, the structural, electronic, elastic, mechanical, and optical properties of K_2CuX (X = As, Sb) ternary compounds were theoretically investigated.[13] This study demonstrated that K_2CuX (X = As, Sb) is mechanically stable, ductile, and ionic. In addition, the optical properties, such as absorption coefficients, established the potential of K_2CuX (X = As, Sb) as a good ultraviolet–visible light absorber desirable for photovoltaic applications.

Despite the growing interest in ternary Zintl-phase materials, K_2AgBi remains largely unexplored, with few experimental reports on its crystal structure properties.[14] To address this knowledge gap, we investigated the structural, electronic, elastic, mechanical, and optical properties of K_2AgBi using a first-principles method for potential optoelectronic applications.

II. COMPUTATIONAL METHODS

Computational analysis of K_2AgBi was carried out using density functional theory (DFT), as implemented in the Quantum ESPRESSO package.[15,16] This approach allows efficient and accurate electronic structure calculations by employing plane wave basis sets and pseudopotential methods to model the interactions between valence electrons and ionic cores.[15] To describe the exchange–correlation interactions, both the local density approximation (LDA) with the Perdew–Zunger (PZ) functional[17] and the generalized gradient approximation (GGA) with the Perdew–Burke–Ernzerhof (PBE) functional[18,19] were initially employed. However, given the limitations of these conventional methods for accurately predicting bandgap values and electronic properties, additional corrections have been introduced using the regularized strongly constrained and appropriately normed (RSCAN) functional[20] and the Tran–Blaha modified Becke–Johnson (TB-mBJ) meta-GGA functional,[21] which have been shown to provide better accuracy for semiconductors and photovoltaic materials.[2]

To effectively model the interaction between the valence electrons and the atomic core, the pseudopotential method was utilized, incorporating two distinct types of pseudopotentials. Ultrasoft (US) pseudopotentials, which include scalar relativistic effects and nonlinear core corrections, were used for standard calculations,[22] whereas norm-conserving pseudopotentials were applied in GGA and meta-GGA simulations to ensure an accurate wavefunction representation.[23] The valence electron configurations of the K_2AgBi system were explicitly considered, with potassium (K) represented as [Ar] $4s^1$, silver (Ag) as [Kr] $5s^1$, and bismuth (Bi) as [Xe] $6s^2$ $6p^3$. Electronic structure and total energy calculations were conducted using the Monkhorst–Pack technique to sample the Brillouin zone (BZ),[24] employing an 11 × 11 × 11 k-point grid with an offset of 1 to optimize computational efficiency and convergence.

Structural optimization was performed through variable cell relaxation under zero external pressure using the Broyden–Fletcher–Goldfarb–Shanno algorithm.[25] The optimization process involved iteratively adjusting the lattice parameters until the total energy reached a minimum, ensuring accurate determination of the equilibrium structural properties. The kinetic energy cutoff for the wave function expansion was fixed at 140.0 Ry, whereas the charge density cutoff was automatically determined based on the system requirements. A stringent convergence criterion of 2.0×10^{-9} Ry was enforced for electronic self-consistency to guarantee numerical accuracy. After the optimized lattice parameters were obtained, self-consistent field (SCF) computations were performed to determine the electronic, mechanical, elastic, and optical properties of the material.

For electronic structure calculations, the same kinetic energy cutoff of 140.0 Ry was employed with an 11 × 11 × 11 k-point grid to ensure accurate electronic band dispersion predictions. To refine the density of states (DOS) evaluations, non-self-consistent field (NSCF) computations were performed using a dense k-point grid of 18 × 18 × 18. The optical properties were determined by computing the complex dielectric function, from which the refractive index, extinction coefficient, absorption coefficient, reflectivity, and energy loss function were derived using the Kramers–Kronig transformation.[26] Post-processing methods from the Quantum ESPRESSO suite were used to analyze these results to enable a thorough assessment of the K_2AgBi potential in photovoltaic and optoelectronic applications.

III. RESULTS AND DISCUSSION

A. Structural properties

K_2AgBi crystallizes in an orthorhombic structure, classified under the *Cmcm* space group (No. 63). The unit cell consisted of lattice parameters determined through structural optimization, with atomic positions assigned to specific Wyckoff sites: Ag at the 4b position with coordinates (1/2, 0.999 357, 3/4), Bi at the 4c site with coordinates (0.228 742, 0, 1/2), and K at the 8 g site with coordinates (0.346 342, 0.327 329, 1/2). The optimized lattice parameters were obtained using the Birch–Murnaghan equation

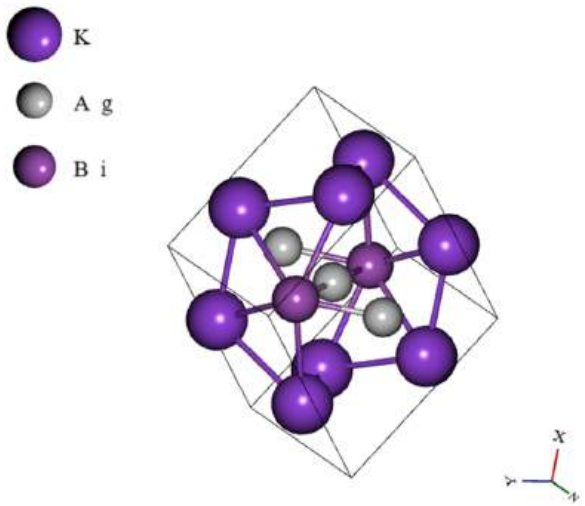

FIG. 1. K_2AgBi crystal structure in its primitive state.

of state [Eq. (1)],[27] which describes the relationship between the total energy and the unit cell volume. The structural arrangement of the K_2AgBi unit cell is shown in Fig. 1, which illustrates its crystallographic configuration. The fitting results using the GGA-PBE and PZ-LDA functionals, shown in Fig. 2, produced characteristic U-shaped energy–volume curves, indicative of equilibrium conditions where the total energy is minimized at an optimal lattice volume,

$$E(V) = E_o + \frac{B}{B'(B'-1)}\left[V\left(\frac{V_o}{V}\right)^{B'} - V_o\right] + \frac{B}{B'}(V - V_o), \quad (1)$$

where E_o, B, B', V, and V_o are the optimum values of the total energy, bulk modulus, pressure derivative of the bulk modulus, total unit-cell volume, and optimized unit-cell volume, respectively.

The computed lattice constants, bulk modulus, and equilibrium volume values revealed key differences between the two functionals, with PBE-GGA consistently predicting larger lattice parameters and equilibrium volumes than PZ-LDA, which tends to overbind, resulting in smaller equilibrium volumes and higher bulk modulus values. Compared to experimental lattice parameters of 19.9467 a.u. (Savelsberg and Schäfer), the PBE-GGA result (20.3333 a.u.) was slightly overestimated, whereas the LDA-PZ value (19.5449 a.u.) was closer to that of the experimental measurement.

The bulk modulus, a measure of the resistance of the material to compression, was significantly higher for the LDA-PZ functional (28.1 GPa) than for PBE-GGA (20.0 GPa), further reinforcing the ability of LDA to predict stiffer materials. The enthalpy of formation calculations suggests that the GGA-PBE functional predicts a more thermodynamically stable structure (−735.55 kJ/mol) than

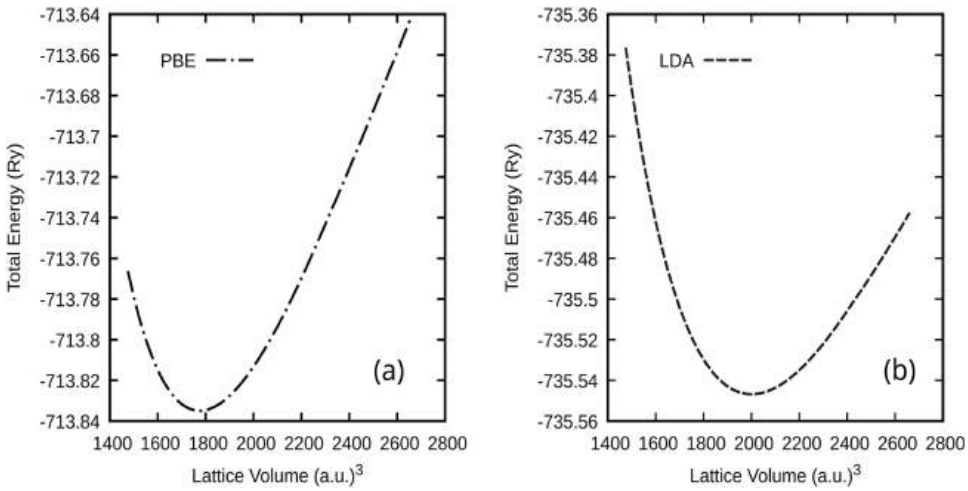

FIG. 2. Birch–Murnaghan fitted total energy as a function of the crystal lattice volume for (a) PBE and (b) LDA.

TABLE I. Calculated ground-state lattice parameters, bulk modulus, equilibrium volumes, and enthalpies of formation of K_2AgBi using PBE and LDA functionals.

	Lattice parameter, a_0 (a.u.)	Bulk modulus, B_0 (GPa)	Equilibrium volume $(a.u.)^3$	Enthalpy of formation, ΔHf (Ry)
PBE	20.3333	20.0	2000.09	−735.55
PZ	19.5449	28.1	1768.80	−713.83
Experiment	19.9467[14]			

LDA-PZ (−713.83 kJ/mol). These findings underscore the importance of selecting an appropriate exchange–correlation functional for DFT calculations, as this choice can influence the prediction of mechanical and structural stability, impacting the assessment of materials for practical applications. The computed structural properties are listed in Table I.

B. Electronic properties

The electronic structure of a material determines its conductivity, optical behavior, and potential applications in semiconductor devices.[28] Electronic structure calculations for the K_2AgBi ternary compounds were conducted using multiple functionals, including GGA-PBE, PZ-LDA, RSCAN, and TB-mBJ, providing comparative

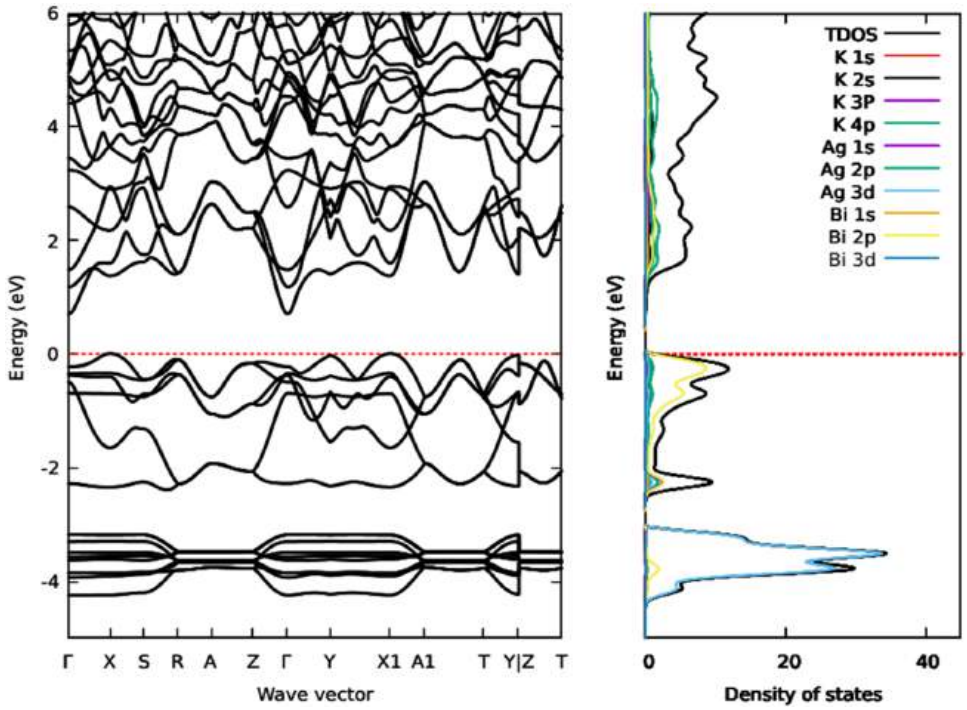

FIG. 3. PBE-GGA band structure and the projected density of states of K_2AgBi showing a bandgap of 0.7848 eV and band formation states.

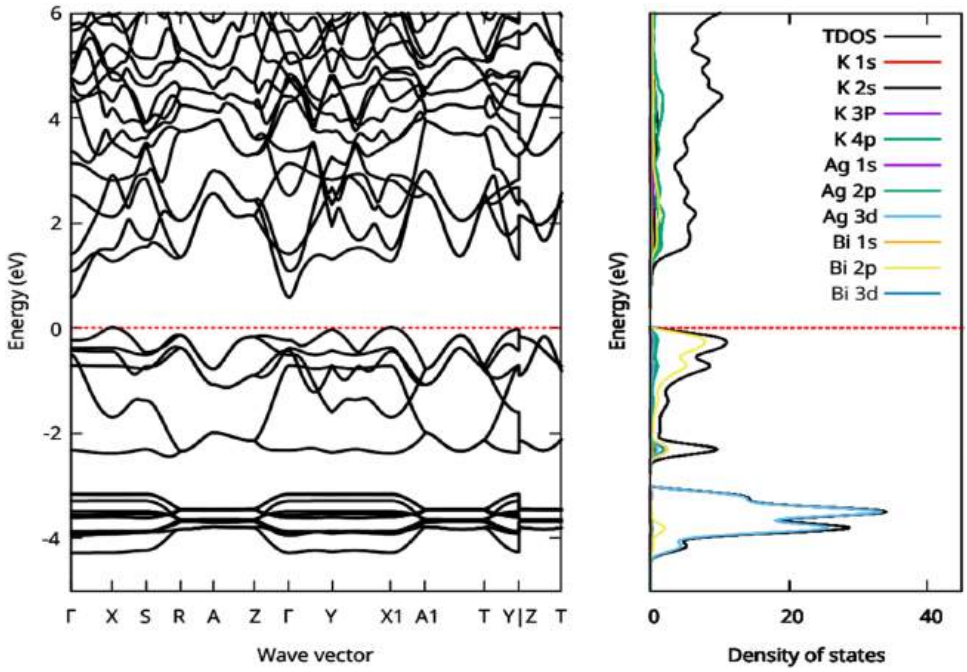

FIG. 4. PZ-LDA band structure and the projected density of states of K_2AgBi showing a bandgap of 0.6732 eV and band formation states.

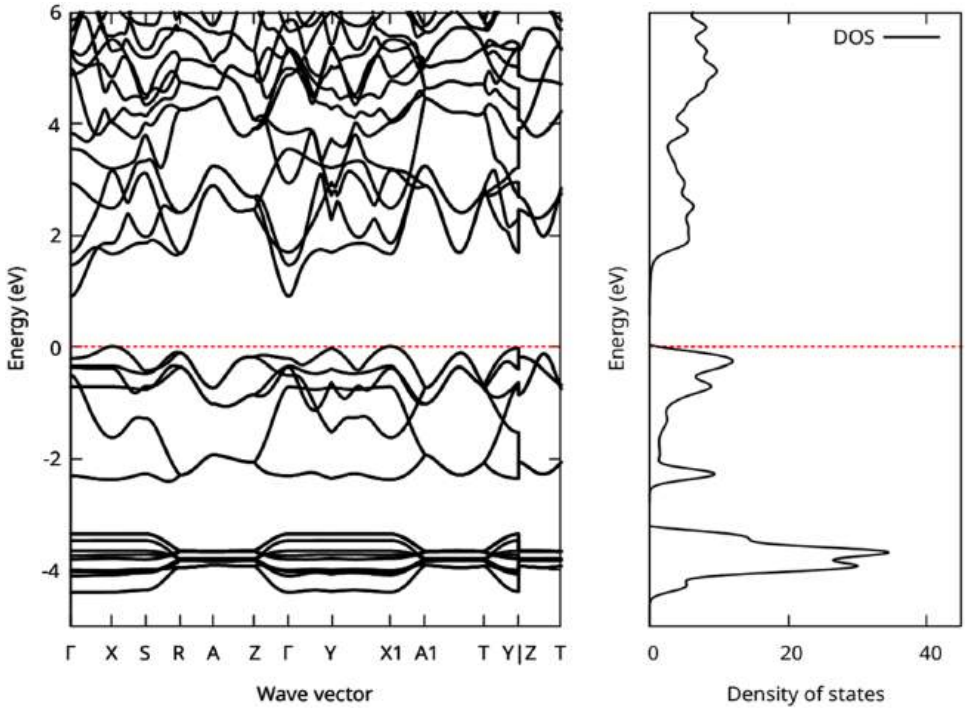

FIG. 5. RSCAN band structure and the projected density of states of K_2AgBi showing a bandgap of 0.9778 eV.

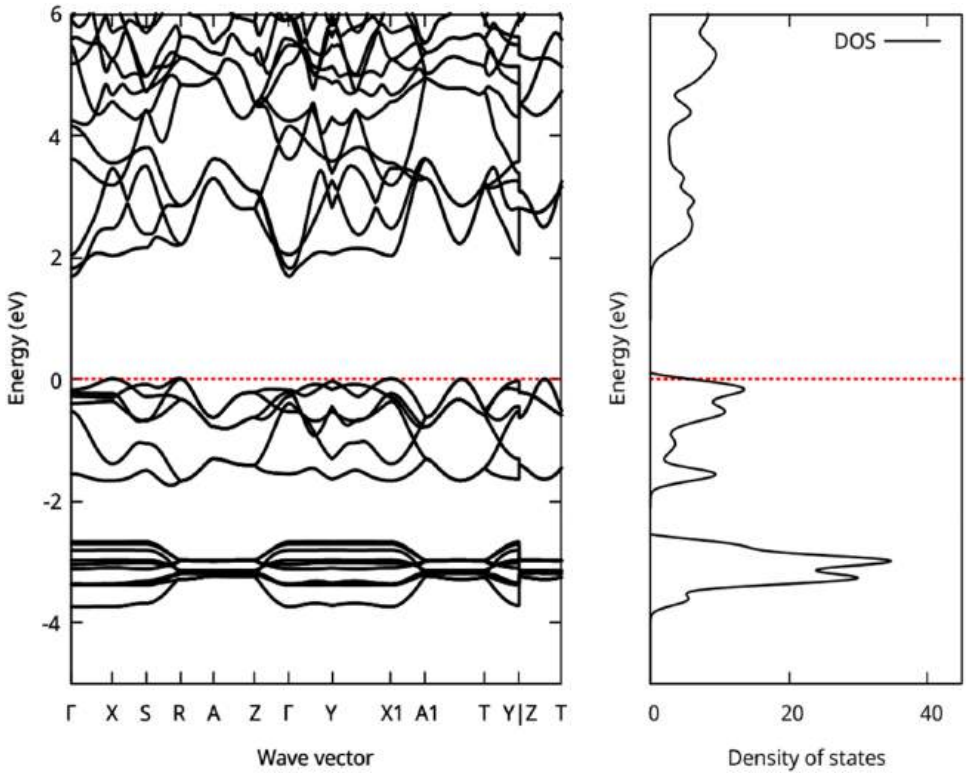

FIG. 6. TB-mBJ band structure and the projected density of states of K_2AgBi showing a bandgap of 0.9346 eV.

TABLE II. Summary of the calculated electronic bandgaps of K_2AgBi using PBE, LDA, RSCAN, and TB-mBJ methods.

	PBE	LDA	RSCAN	TB-mBJ
This work	0.7868 eV	0.6732 eV	0.9778 eV	0.9346 eV

insights into the electronic band dispersion and density of states. The computed bandgap values indicate that the K_2AgBi ternary compound is a narrow-gap semiconductor, with the PBE-GGA functional yielding a bandgap of 0.7848 eV (Fig. 3). PZ-LDA predicts a slightly smaller bandgap of 0.6732 eV (Fig. 4), consistent with LDA's tendency to underestimate the bandgap.[29] The projected density of states (PDOS) analysis revealed that the valence band is primarily formed by the Ag 3*d*, Bi 2*p*, and K 1*s* orbitals, whereas the conduction band is mainly formed by the K 4*p*, Ag 2*p*, and K 2*s* orbitals. The sharper peaks in the PDOS obtained using PZ-LDA indicate more localized states, whereas those obtained using PBE-GGA suggest a broader distribution, implying more delocalized electronic states. To refine the bandgap predictions, meta-GGA functionals were employed, with RSCAN yielding a bandgap of 0.9778 eV (Fig. 5) and TB-mBJ predicting a bandgap of 0.9346 eV (Fig. 6). The conduction band minimum (CBM) of the K_2AgBi ternary compound appeared at the Γ point, whereas the valence band maximum (VBM) appeared at the X symmetry point, revealing an indirect bandgap.[30] Because the pseudopotentials utilized in meta-GGA methods do not have the required orbitals for projection, the electronic band structures obtained using meta-GGA methods are shown without the appropriate projected density of states.[2] These results highlight the improved accuracy of meta-GGA functionals over the conventional GGA and LDA approximations in electronic structure calculations. The computed bandgap values for all the functionals are summarized in Table II.

C. Mechanical and elastic properties

The mechanical stability of a material is critical for its practical application, particularly in photovoltaic and electronic devices, where mechanical resilience is required.[31] The K_2AgBi compound, with its orthorhombic crystal symmetry, has a full set of nine independent elastic constants (C_{11}, C_{12}, C_{13}, C_{22}, C_{23}, C_{33}, C_{44}, C_{55}, and C_{66}), which determine its response to external stresses (Table III). The Born stability criteria for orthorhombic systems,[32] expressed in the following equation, confirm that the computed elastic constants satisfy the mechanical stability conditions, indicating that K_2AgBi is mechanically stable:

$$\begin{gathered} C_{11} > 0, C_{11}C_{22} > C_{12}^2, \\ C_{11}C_{22}C_{33} + 2C_{12}C_{13}C_{23} - C_{11}C_{23}^2 - C_{22}C_{13}^2 - C_{33}C_{12}^2 > 0, \\ C_{44} > 0, C_{55} > 0, C_{66} > 0. \end{gathered} \tag{2}$$

The Voigt–Reuss–Hill averaging method[33] was used to determine the bulk modulus (B), shear modulus (G), and Young's modulus (E), with the values of B = 14.81 GPa, G = 7.84 GPa, and E = 19.96 GPa using the PBE-GGA functional, with slightly lower values from the LDA-PZ approximation (Table IV). Pugh's ratio (B/G) is a key metric for classifying materials as brittle or ductile, where B/G values above 1.75 indicate ductility. The computed B/G ratios of 1.89 (PBE-GGA) and 1.67 (LDA-PZ) suggest that K_2AgBi is ductile, which is advantageous for applications requiring flexibility and mechanical resilience.

TABLE III. Elastic constants in GPa for the K_2AgBi crystal system.

	C_{11}	C_{12}	C_{13}	C_{22}	C_{23}	C_{33}	C_{44}	C_{55}	C_{66}
PBE	31.45	8.88	4.28	28.18	14.45	24.02	14.38	6.38	3.96
LDA	25.92	4.74	1.95	20.96	11.09	20.39	15.99	5.68	2.66

TABLE IV. Voigt–Reuss–Hill average mechanical properties: B, E, G, Pugh's ratio (B/G), Poisson's ratio (n), Kleinman parameter (ζ), and Debye temperature (θ_D) of the K_2AgBi ternary compound.

	B	E	G	B/G	*n*	ζ	θ_D (K)
PBE	14.81	19.96	7.84	1.89	0.2730	1.498	129.5
LDA	11.36	16.96	6.82	1.67	0.2435	1.689	117.9

Poisson's ratio results (Table IV) suggest that K_2AgBi exhibits ionic bonding, which is a key feature of Zintl-phase materials. The PZ-LDA value (n = 0.2435) is near the covalent–ionic threshold, whereas GGA-PBE (n = 0.2730) falls within the ionic range ($0.25 < n < 0.5$).[34] The tendency of LDA to underestimate the lattice constants and overbind atoms likely results in a lower Poisson's ratio, making the PBE value more reliable. Because PBE places K_2AgBi in the ionic range, this supports its predominantly ionic character. Further validation through charge transfer analysis and electronic structure calculations could strengthen this conclusion.

The Kleinman parameter ζ describes the anisotropic or isotropic nature of a material, which is calculated using the following equation:[2,35]

$$\varsigma = \frac{C_{33}(C_{11} + C_{22}) - 2C_{23}^2}{C_{11}C_{22} - C_{23}^2}. \tag{3}$$

A material is considered isotropic if ζ = 1, or anisotropic if ζ > 1. For K_2AgBi, which has an orthorhombic structure, the Kleinman parameters were calculated to be 1.498 and 1.689 using the PBE and LDA (Table IV), respectively, indicating that the material is anisotropic. Furthermore, the spatial dependence of the mechanical properties of the K_2AgBi ternary compound, as depicted in Fig. 7, provides insights into the anisotropy of Young's modulus, shear modulus, and Poisson's ratio across different crystallographic planes.[36] The Young's modulus plots [Fig. 7(a)] indicate significant anisotropy because the green contours exhibit a directional dependence in all three planes (xy, xz, and yz). This suggests that the stiffness of the material varies depending on the crystallographic orientation, which has implications for its mechanical stability and potential applications in which directional mechanical properties are critical. The shear modulus plots [Fig. 7(b)] further reinforce this anisotropy, with the blue contours representing isotropic regions and the green contours capturing the variations in the shear response of the material. The presence of distinct lobes in different planes indicates

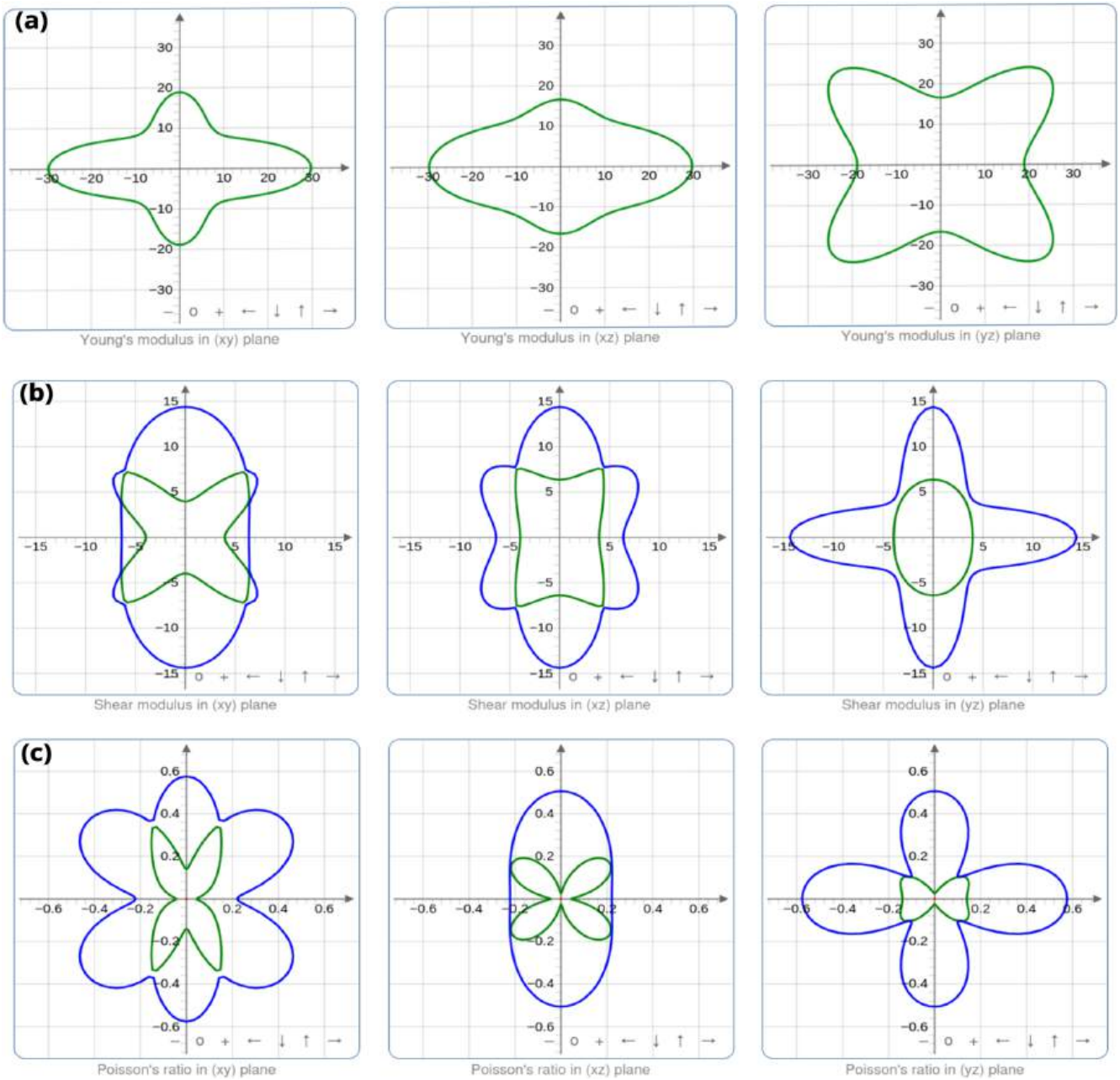

FIG. 7. Spatial dependence of the mechanical properties: (a) Young's modulus, (b) shear modulus, and (c) Poisson's ratio of the K_2AgBi ternary compound.

a directional dependence on the resistance of the material to shear deformation.

The Poisson's ratio plots [Fig. 7(c)] highlight the extent of elastic deformation and coupling between the strain components in different directions. The blue curves represent anisotropy, whereas the green and red curves indicate the regions of positive and negative linear compressibility, respectively. The variation in Poisson's ratio suggests that the material exhibits unique deformation characteristics under mechanical stress, including possible auxetic behavior (negative Poisson's ratio) in certain directions. Overall, these mechanical property maps emphasize the importance of considering anisotropy when designing applications where K_2AgBi is used, particularly in mechanical, electronic, and thermoelectric devices that require tailored elastic properties.

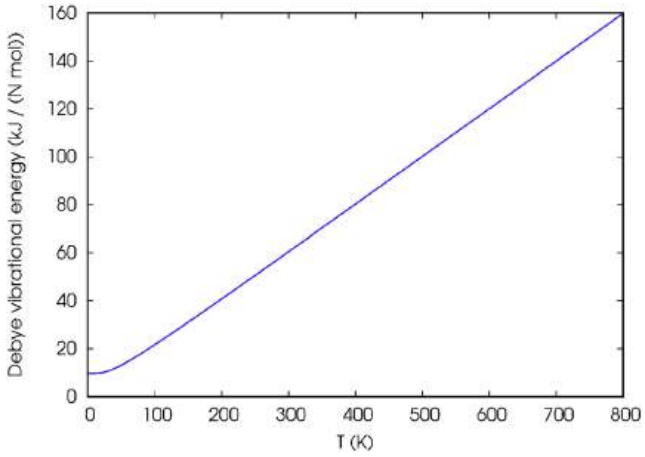

FIG. 8. Debye vibrational energy of the K_2AgBi ternary compound as a function of temperature.

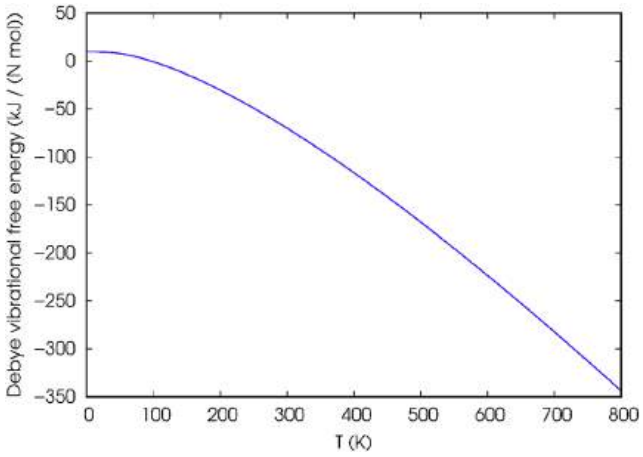

FIG. 9. Debye vibrational free energy of the K_2AgBi ternary compound as a function of temperature.

The thermophysical behavior of the K_2AgBi ternary compound was analyzed using Debye theory, which describes the vibrational properties of crystalline solids at finite temperatures.[37] The Debye temperature is a key parameter influencing thermal expansion, heat capacity, and lattice vibrations. The Debye vibrational energy of the K_2AgBi ternary compound, as shown in Fig. 8, exhibited a characteristic temperature dependence consistent with the Debye model of lattice vibrations. At low temperatures, the vibrational energy increases nonlinearly because of quantum effects that limit the phonon population at low thermal energies. As the temperature increases, the energy curve transitions to a nearly linear behavior, reflecting the classical limit where the vibrational energy follows the Dulong–Petit law. This trend suggests that the phonon contribution to the thermodynamic properties of the material becomes significant as the temperature increases, influencing its heat capacity and thermal expansion. The steady increase in vibrational energy indicates that the material maintains a predictable phononic response over the investigated temperature range, which is crucial for understanding its thermal stability and its potential applications in thermoelectric or optoelectronic devices. Moreover, the observed behavior aligns with typical Debye theory predictions for crystalline solids, suggesting that K_2AgBi follows standard phonon dynamics without anomalous soft modes or strong anharmonic effects at the studied temperature.

The Debye vibrational free energy of the K_2AgBi ternary compound, as depicted in Fig. 9, exhibited a characteristic decrease with increasing temperature, which is consistent with the thermodynamic behavior predicted by the Debye model. At low temperatures, the free energy starts near zero and decreases gradually owing to the influence of quantum mechanical effects, which dominate the phonon contributions at lower thermal energies. As the temperature increased, the free energy decreased more rapidly, reflecting the increasing vibrational entropy and the corresponding reduction in the Helmholtz free energy. This trend is significant for understanding the thermal stability of the material, as a lower free energy at higher temperatures indicates enhanced phonon contributions to the system's entropy and heat capacity. The concave nature of the curve suggests that phonon excitations play a major role in determining thermodynamic properties, which is particularly relevant for applications in thermal and electronic transport. The observed behavior aligns well with the standard Debye theory predictions for crystalline solids, reaffirming that K_2AgBi follows the expected lattice dynamics without exhibiting anomalous anharmonic effects or phase transitions in the examined temperature range. These insights are critical for evaluating the material's thermodynamic performance, particularly in applications requiring high-temperature stability and efficient thermal management.

Figure 10 shows the Debye heat capacity of the K_2AgBi ternary compound. A high heat capacity indicates high thermal conductivity and low thermal diffusivity in the material.[2,38] This figure shows a rapid increase in the heat capacity before leveling off to a nearly constant value. This behavior aligns with predictions from the Debye model, which states that heat capacity stabilizes at a constant value after reaching the material's Debye temperature,[39] previously determined in the elastic constant calculation as θ_D = 129.5 K using the GGA-PBE method and θ_D = 117.9 K using the LDA-PZ method (Table IV).

D. Optical properties

The optical response of K_2AgBi was analyzed using the frequency-dependent dielectric function [Eq. (4)], refractive index [Eq. (5)], extinction coefficient [Eq. (6)], reflectivity [Eq. (7)], absorption coefficient [Eq. (8)], and energy loss function [Eq. (9)],[40,41]

$$\varepsilon(\omega) = \varepsilon_1(\omega) + \varepsilon_2(\omega), \tag{4}$$

$$n(\omega) = \sqrt{\frac{\sqrt{\left(\varepsilon_1^2(\omega) + \varepsilon_2^2(\omega)\right)} + \varepsilon_1(\omega)}{2}}, \tag{5}$$

$$\kappa(\omega) = \sqrt{\frac{\sqrt{\left(\varepsilon_1^2(\omega) + \varepsilon_2^2(\omega)\right)} - \varepsilon_1(\omega)}{2}}, \tag{6}$$

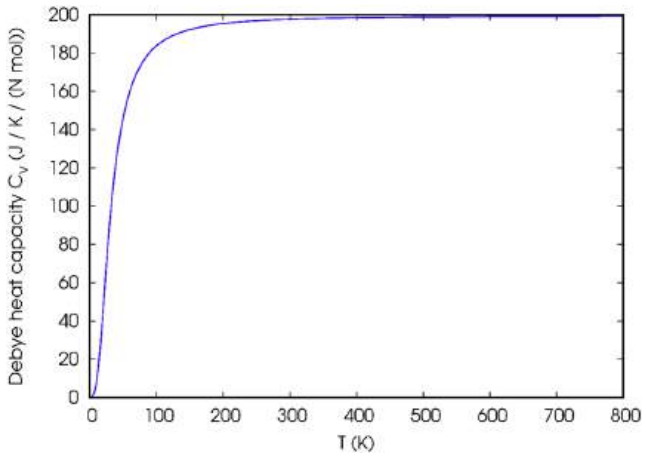

FIG. 10. Debye heat capacity of the K_2AgBi ternary compound as a function of temperature.

$$R(\omega) = \frac{(n(\omega)-1)^2 + \kappa^2(\omega)}{(n(\omega)+1)^2 + \kappa^2(\omega)}, \tag{7}$$

$$\alpha(\omega) = \frac{2\omega k}{c}, \tag{8}$$

$$L(\omega) = \frac{\varepsilon_2(\omega)}{\varepsilon_1^2(\omega) + \varepsilon_2^2(\omega)}, \tag{9}$$

where $\varepsilon_1(\omega) = n^2(\omega) - \kappa^2(\omega)$ is the real part, while $\varepsilon_2(\omega) = 2n\kappa$ is the imaginary part of the dielectric function. The dielectric functional components of the K_2AgBi ternary compound are shown in Fig. 11. The real part, ε_1, represents the ability of the material to store electrical energy and is crucial for understanding the refractive-index behavior, whereas the imaginary part, ε_2, corresponds to the absorption and electron excitation processes. The peak in ε_2 at lower photon energies suggests strong interband transitions, which are likely associated with the electronic excitation from the valence band to the conduction band. The sharp initial increase in ε_2, followed by a gradual decline at higher energies, indicates that the absorption is most significant in the low-energy region and decreases as the photon energy increases. The behavior of ε_1 showed a corresponding peak and subsequent decline, followed by a steady region at higher energies, which is indicative of dielectric screening effects. The point at which ε_1 crosses zero marks a crucial transition that typically corresponds to the plasma frequency, which influences the reflectivity and transparency at different energy ranges. Because of its significant optical absorption in the visible and near-infrared (NIR) spectra, K_2AgBi may find potential applications in optoelectronic devices, such as photodetectors and solar cells.

The frequency dependent refractive index (n) and extinction coefficient (κ) of the K_2AgBi ternary compound shown in Fig. 12 provide valuable insights into its optical response across different photon energies. The refractive index (n) describes the speed of light propagation in a material and is crucial for understanding its transparency and dispersion characteristics. Conversely, the extinction coefficient quantifies the absorption of incident light by the material and is directly related to optical losses. At lower photon energies, the refractive index (n) exhibited a peak, indicating strong dispersion effects in the material. This behavior suggests that K_2AgBi exhibits

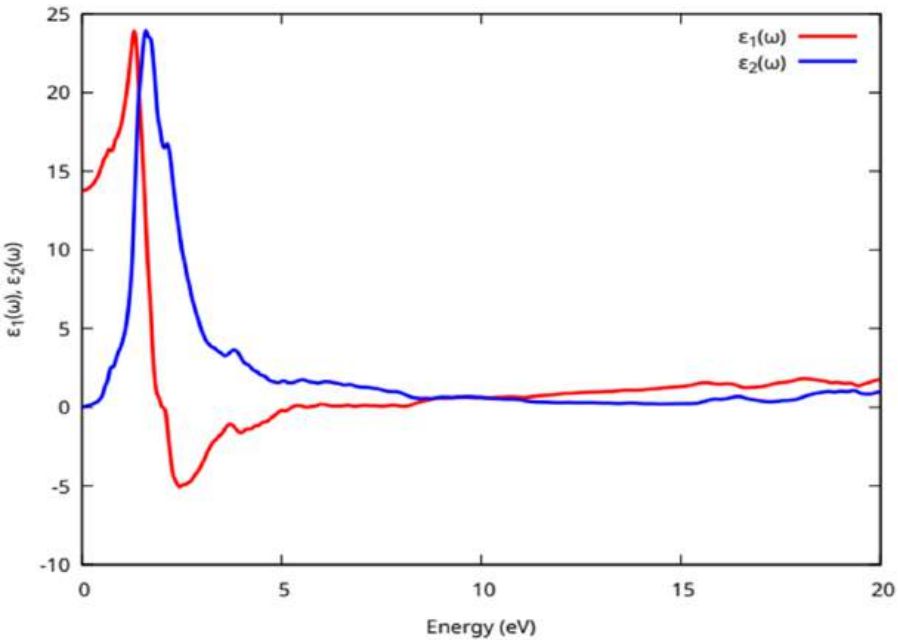

FIG. 11. Dielectric constants ε_1 and ε_2 of the K_2AgBi ternary compound.

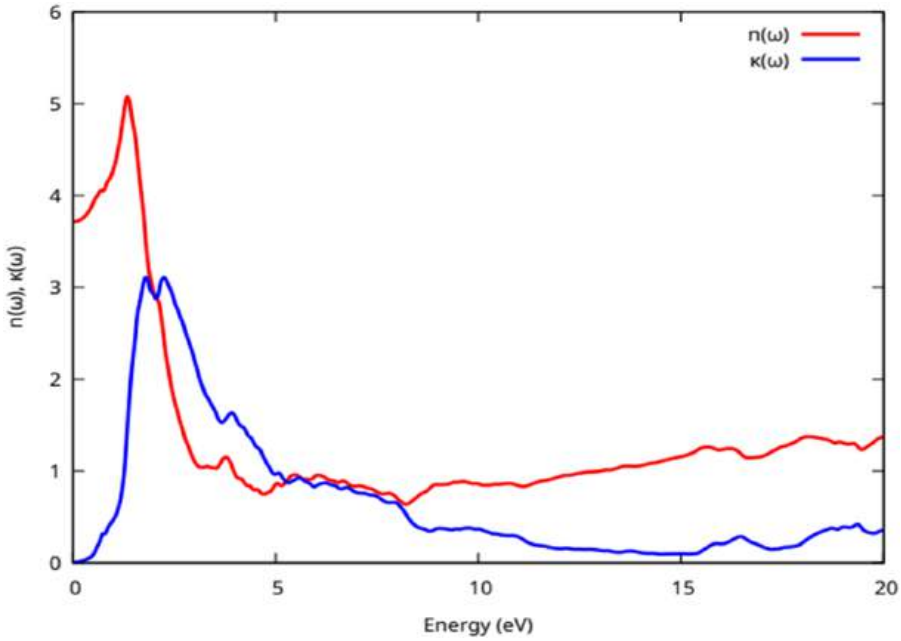

FIG. 12. Frequency-dependent refractive index and extinction coefficient of the K_2AgBi ternary compound.

significant light-bending properties in this energy region, indicating its potential for use in optoelectronics. As the photon energy increased, n gradually decreased, reaching a relatively stable region at higher energies, indicating a reduced dispersion. The extinction coefficient κ follows a trend similar to that of the imaginary part of the dielectric function (ε_2), showing a strong peak at low photon energies, which corresponds to significant optical absorption owing to interband transitions. The decrease in κ at higher photon energies suggests a reduced absorption, which allows more light to pass through the material. The interplay between n and κ determines the reflectivity and transmissivity of K_2AgBi, making these properties essential for designing materials for photonic and electronic

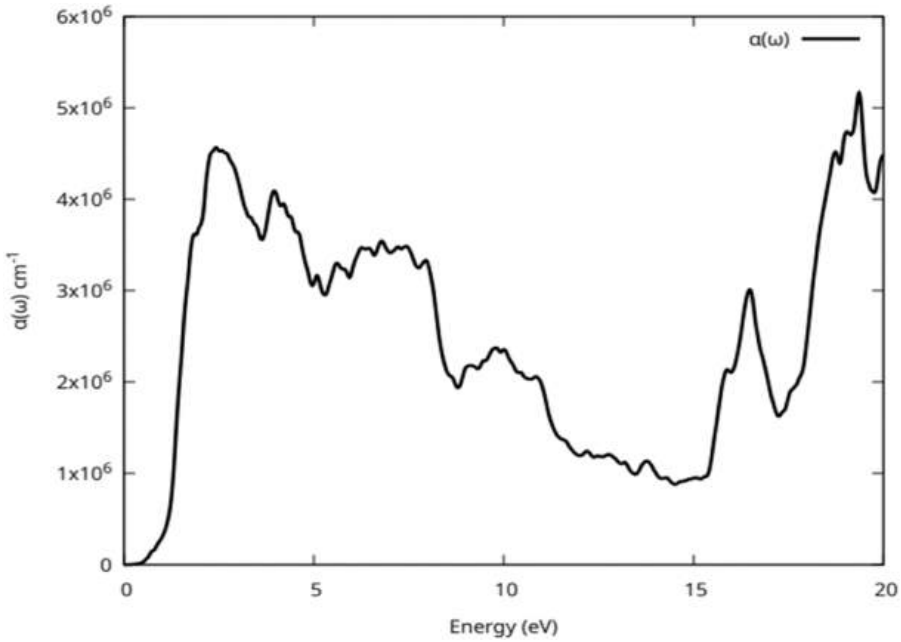

FIG. 13. Frequency-dependent absorption coefficient of the K_2AgBi ternary compound.

applications. Overall, the observed optical behavior indicates that K_2AgBi has potential for use in optoelectronic devices, particularly in applications where controlled absorption and refractive index tuning are required.

The frequency-dependent absorption coefficient of the K_2AgBi ternary compound, depicted in Fig. 13, provides crucial insights into its optical absorption behavior across different photon energies. The absorption coefficient (α) determines how strongly the material absorbs incident light, making it a key parameter for optoelectronic applications, such as photodetectors, solar cells, and light-emitting devices. As shown in the imaginary component of the dielectric function (ε_2) and extinction coefficient, κ, the figure displays a notable absorption peak in the low-energy region, which corresponds to strong electronic transitions from the valence band to the conduction band. This suggests that K_2AgBi has strong interband absorption near its fundamental bandgap, making it an efficient absorber in the visible-to-near-infrared (NIR) spectrum. As the photon energy increased, the absorption coefficient gradually declined, indicating a reduction in the available electronic transitions and suggesting that higher-energy photons experience lower absorption. The rapid increase at lower photon energies is characteristic of a direct or weakly indirect bandgap material, where electronic transitions occur efficiently without significant phonon contributions. The absorption edge observed in the plot provides an estimate of the optical bandgap, which is critical for determining the suitability of the material for photovoltaic and semiconductor applications. Overall, the absorption spectrum indicates that K_2AgBi has strong light-harvesting capabilities in specific energy ranges, reinforcing its potential use in optoelectronic applications that require high absorption efficiency.

The frequency-dependent energy loss function of the K_2AgBi ternary compound shown in Fig. 14 provides insights into its plasmonic behavior and electron energy dissipation mechanisms. A pronounced peak in the energy-loss function corresponds to the plasma frequency, where the real part of the dielectric function (ε_1) crosses zero, indicating a strong plasmonic resonance and collective electron oscillations. At lower frequencies, the minimal energy loss suggests dominant interband transitions, whereas the sharp peak at higher frequencies indicates significant electron excitation and energy dissipation. This behavior is crucial for understanding the optical and electronic properties of K_2AgBi, particularly in plasmonic and photonic applications, where controlled energy loss can influence performance. The presence of a well-defined plasmon peak suggests that K_2AgBi exhibits metallic-like optical properties in specific frequency ranges, making it a promising material for applications in optical coatings, energy conversion, and plasmonic-based technologies.

The frequency-dependent reflectivity of the K_2AgBi ternary compound shown in Fig. 15 provides essential insights into its optical response and surface interactions with electromagnetic radiation. The reflectivity spectrum exhibited a significant increase at lower frequencies, indicating strong optical reflection owing to interband transitions and possible metallic-like behavior in this region. As the frequency increases, the reflectivity gradually decreases, suggesting enhanced light absorption and reduced reflection, which aligns with the observed trends in the absorption coefficient and dielectric function. A sharp drop in reflectivity at higher frequencies corresponds to the plasma frequency, where free carriers transition from reflective to transmissive behavior. This characteristic is crucial for applications in optical coatings, photonic devices, and plasmonic materials, where controlled reflectivity plays a key role

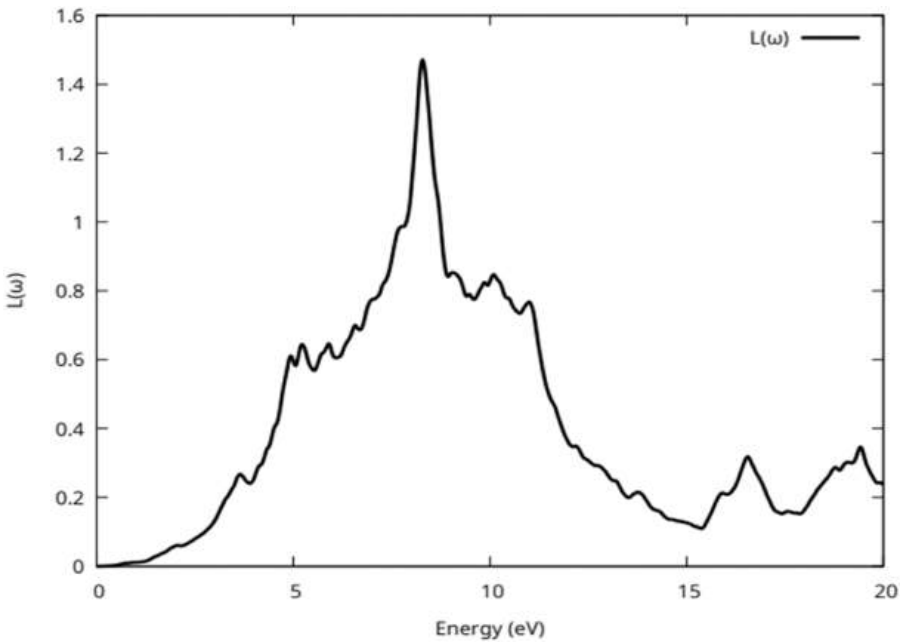

FIG. 14. Frequency-dependent energy loss function of the K_2AgBi ternary compound.

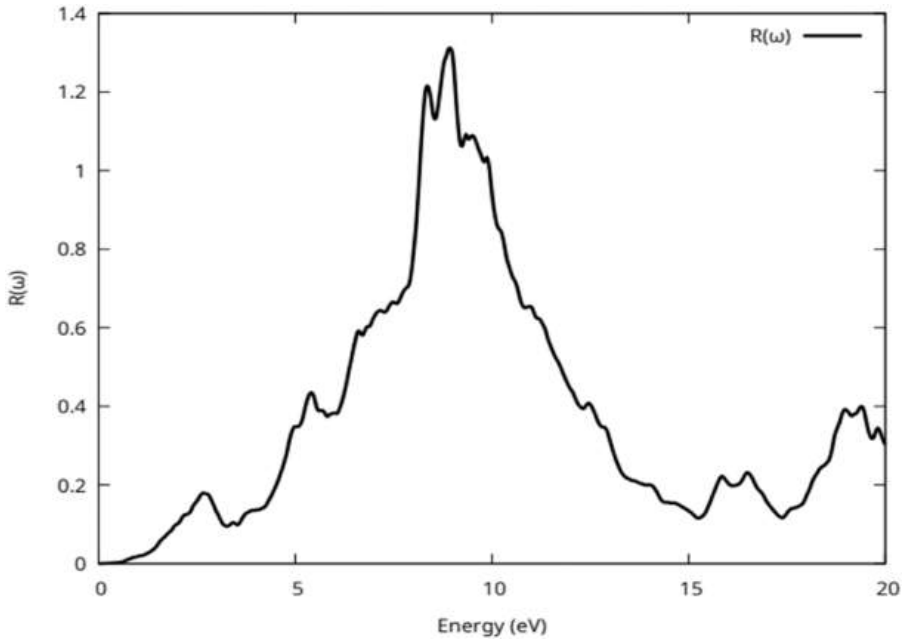

FIG. 15. Frequency-dependent reflectivity of the K_2AgBi ternary compound.

in the device performance. The overall trend suggests that K_2AgBi has the potential for applications requiring tunable reflectance, such as energy-efficient coatings, infrared shielding, or optoelectronic devices.

IV. CONCLUSION

First-principles investigation of the properties of the K_2AgBi ternary compound was carried out to establish its potential for optoelectronic applications. The negative formation energies confirm the thermodynamic stability of the K_2AgBi ternary compound. Electronic bandgaps of 0.6732 eV (PZ-LDA), 0.7848 eV (PBE-GGA), 0.9346 eV (TB-mBJ), and 0.9778 eV (RSCAN) were obtained, which are desirable for optoelectronic device applications. The K_2AgBi material was shown to be mechanically stable based on the elastic constant analysis. The K_2AgBi ternary compound exhibited mechanical ductility, anisotropic elastic behavior, and ionic bonding, consistent with its Zintl-phase classification. Optical analysis revealed strong absorption in the visible to ultraviolet range, supporting its potential for photovoltaic applications. In addition, the computed thermal properties suggest stable phononic behavior, making K_2AgBi a promising candidate for energy and optoelectronic technologies.

ACKNOWLEDGMENTS

The authors acknowledge the Tanzanian Higher Education for Economic Transformation Project (HEET-PROJECT No. P 166415) for the financial support and the Centre for High Performance Computing (CHPC-RSA) for computational resources.

AUTHOR DECLARATIONS

Conflict of Interest

The authors have no conflicts to disclose.

Author Contributions

John Peter Kachira: Conceptualization (equal); Data curation (equal); Formal analysis (equal); Investigation (equal); Methodology (equal); Writing – original draft (equal); Writing – review & editing (equal). **Robinson Musembi**: Conceptualization (equal); Data curation (equal); Formal analysis (equal); Funding acquisition (equal); Investigation (equal); Methodology (equal); Project administration (equal); Resources (equal); Software (equal); Supervision (equal); Validation (equal); Visualization (equal); Writing – original draft (equal); Writing – review & editing (equal). **Francis Nyongesa**: Conceptualization (equal); Data curation (equal); Formal analysis (equal); Resources (equal); Supervision (equal); Writing – original draft (equal); Writing – review & editing (equal). **Mwende Mbilo**: Conceptualization (equal); Data curation (equal); Investigation (equal); Validation (equal); Visualization (equal); Writing – original draft (equal); Writing – review & editing (equal). **Martin Nyamuga**: Data curation (equal); Investigation (equal); Methodology (equal); Validation (equal); Visualization (equal); Writing – original draft (equal); Writing – review & editing (equal). **Ibrahim Musanyi**: Data curation (equal); Investigation (equal); Methodol-

ogy (equal); Validation (equal); Writing – original draft (equal); Writing – review & editing (equal).

DATA AVAILABILITY

The data that support the findings of this study are available from the corresponding author upon reasonable request.

REFERENCES

[1] L. Panagoda, R. Sandeepa, W. Perera, D. M. I. Sandunika, S. Siriwardhana, M. Alwis, and S. H. S. Dilka, "Advancements in photovoltaic (Pv) technology for solar energy generation," J. Res. Technol. Eng. **4**(30), 30–72 (2023) https://www.jrte.org/wp-content/uploads/2023/07/Advancements-In-Photovoltaic-Pv-Technology-for-Solar-Energy-Generation.pdf.

[2] R. Musembi, M. Mbilo, M. Nyamunga, and J. Kachila, "Analysis of Na_2CuP ternary semiconductor compound for optoelectronic application by first-principles methods using GGA and mGGA functionals," Comput. Condens. Matter **40**, e00927 (2024).

[3] M. M. Kimuyu, R. Musembi, J. Mwabora, and F. Nyongesa, "New findings on a Zintl phased $K_3Ag_3As_2$ ternary semiconductor compound for photovoltaic applications by first-principles methods," Mater. Adv. **5**(4), 1639–1647 (2024).

[4] C. Ballif, F.-J. Haug, M. Boccard, P. J. Verlinden, and G. Hahn, "Status and perspectives of crystalline silicon photovoltaics in research and industry," Nat. Rev. Mater. **7**(8), 597–616 (2022).

[5] S. Wafula, R. Musembi, and F. Nyongesa, "Analysis of K_4ZnAs_2 Zintl phased ternary semiconductor compound for optoelectronic application," Results Mater. **20**, 100469 (2023).

[6] M. A. Scarpulla, B. McCandless, A. B. Phillips, Y. Yan, M. J. Heben, C. Wolden, G. Xiong, W. K. Metzger, D. Mao, D. Krasikov *et al.*, "CdTe-based thin film photovoltaics: Recent advances, current challenges and future prospects," Sol. Energy Mater. Sol. Cells **255**, 112289 (2023).

[7] T. Schmiermund, *The Discovery of the Periodic Table of the Chemical Elements: A Short Journey from the Beginnings Until Today* (Springer Fachmedien Wiesbaden, Wiesbaden, 2022).

[8] T. F. Fässler, *Zintl Phases: Principles and Recent Developments* (Springer, Berlin, Heidelberg, 2011).

[9] L. M. Shaker, A. Al-Amiery, and W. N. R. W. Isahak, "Optoelectronics' quantum leap: Unveiling the breakthroughs driving high-performance devices," Green Technol. Sustainability **2**, 100111 (2024).

[10] I. Ghazal, H. Absike, A. Rachadi, and H. Ez-Zahraouy, "Investigation of the electronic, structural, optical and thermoelectric properties of ternary chalcopyrite $ACuS_2$(A = Al, Ga and In): Ab initio study," Optik **260**, 169077 (2022).

[11] A. Ovchinnikov and S. Bobev, "Zintl phases with group 15 elements and the transition metals: A brief overview of pnictides with diverse and complex structures," J. Solid State Chem. **270**, 346–359 (2019).

[12] R. Musembi and M. Mbilo, "Computational study on structural, elastic, mechanical and optical properties of K_2AgAs ternary semiconductor compound," AIP Adv. **13**(11), 115218 (2023).

[13] M. Mbilo and R. Musembi, "First-principle calculations to investigate structural, electronic, elastic, mechanical, and optical properties of K_2CuX (X = As, Sb) ternary compounds," Adv. Mater. Sci. Eng. **2022**, 1–10.

[14] G. Savelsberg and H. Schäfer, "Darstellung und kristallstruktur von Na_2CuP, K_2AgAs, K_2AgSb und K_2AgBi/preparation and crystal structure of Na_2CuP, K_2AgAs, K_2AgSb, and K_2AgBi," Z. Naturforsch., B **32**(7), 745–748 (1977).

[15] P. Giannozzi, S. Baroni, N. Bonini, M. Calandra, R. Car, C. Cavazzoni, D. Ceresoli, G. L. Chiarotti, M. Cococcioni, I. Dabo *et al.*, "Quantum ESPRESSO: A modular and open-source software project for quantum simulations of materials," J. Phys.: Condens. Matter **21**(39), 395502 (2009).

[16] P. Giannozzi, O. Andreussi, T. Brumme, O. Bunau, M. Buongiorno Nardelli, M. Calandra, R. Car, C. Cavazzoni, D. Ceresoli, M. Cococcioni *et al.*, "Advanced capabilities for materials modelling with Quantum ESPRESSO," J. Phys.: Condens. Matter **29**(46), 465901 (2017).

[17] S. Goedecker and C. J. Umrigar, "Critical assessment of the self-interaction-corrected-local-density-functional method and its algorithmic implementation," Phys. Rev. A **55**(3), 1765–1771 (1997).

[18] M. Ernzerhof and G. E. Scuseria, "Assessment of the Perdew–Burke–Ernzerhof exchange-correlation functional," J. Chem. Phys. **110**(11), 5029–5036 (1999).

[19] J. P. Perdew, K. Burke, and M. Ernzerhof, "Perdew, Burke, and Ernzerhof reply," Phys. Rev. Lett. **80**(4), 891 (1998).

[20] A. P. Bartók and J. R. Yates, "Regularized SCAN functional," J. Chem. Phys. **150**(16), 161101 (2019).

[21] K. Nakano and T. Sakai, "Assessing the performance of the Tran–Blaha modified Becke–Johnson exchange potential for optical constants of semiconductors in the ultraviolet–visible light region," J. Appl. Phys. **123**(1), 015104 (2018).

[22] G. Kresse and D. Joubert, "From ultrasoft pseudopotentials to the projector augmented-wave method," Phys. Rev. B **59**(3), 1758–1775 (1999).

[23] D. R. Hamann, "Optimized norm-conserving Vanderbilt pseudopotentials," Phys. Rev. B **88**(8), 085117 (2013).

[24] R. A. Evarestov and V. P. Smirnov, "Modification of the Monkhorst-Pack special points meshes in the Brillouin zone for density functional theory and Hartree-Fock calculations," Phys. Rev. B **70**(23), 233101 (2004).

[25] J. D. Head and M. C. Zerner, "A Broyden–Fletcher–Goldfarb–Shanno optimization procedure for molecular geometries," Chem. Phys. Lett. **122**(3), 264–270 (1985).

[26] A. B. Kuzmenko, "Kramers–Kronig constrained variational analysis of optical spectra," Rev. Sci. Instrum. **76**(8), 083108 (2005).

[27] R. Jeanloz, "Universal equation of state," Phys. Rev. B **38**(1), 805–807 (1988).

[28] A. L. Efros and M. Rosen, "The electronic structure of semiconductor nanocrystals," Annu. Rev. Mater. Sci. **30**(1), 475–521 (2000).

[29] S. Kumar, H. Bui, and G. Bester, "Empirical band-gap correction for LDA-derived atomic effective pseudopotentials," Comput. Condens. Matter **40**, e00917 (2024).

[30] L.-D. Yuan, H.-X. Deng, S.-S. Li, S.-H. Wei, and J.-W. Luo, "Unified theory of direct or indirect band-gap nature of conventional semiconductors," Phys. Rev. B **98**(24), 245203 (2018).

[31] F. Song, D. Zheng, J. Feng, J. Liu, T. Ye, Z. Li, K. Wang, S. F. Liu, and D. Yang, "Mechanical durability and flexibility in perovskite photovoltaics: Advancements and applications," Adv. Mater. **36**(18), 2312041 (2024).

[32] F. Mouhat and F.-X. Coudert, "Necessary and sufficient elastic stability conditions in various crystal systems," Phys. Rev. B **90**(22), 224104 (2014).

[33] D. H. Chung and W. R. Buessem, "The Voigt-Reuss-Hill approximation and elastic moduli of polycrystalline MgO, CaF_2, β-ZnS, ZnSe, and CdTe," J. Appl. Phys. **38**(6), 2535–2540 (1967).

[34] G. N. Greaves, A. L. Greer, R. S. Lakes, and T. Rouxel, "Poisson's ratio and modern materials," Nat. Mater. **10**(11), 823–837 (2011).

[35] M. Debbarma, S. Das, B. Debnath, D. Ghosh, S. Chanda, R. Bhattacharjee, and S. Chattopadhyaya, "Density functional calculations of elastic and thermal properties of zinc-blende HgS_xSe_{1-x}, HgS_xTe_{1-x} and $HgSe_xTe_{1-x}$ ternary alloys," Comput. Condens. Matter **24**, e00482 (2020).

[36] M. D. Rafique, M. Awais, F. Gulzar, and S. S. A. Gillani, "First principles computation of insulator–semiconductor–metal transition and its impact on structural, elastic, mechanical, anisotropic and optical properties of $CsSrF_3$ under systematic static isotropic pressure," Mol. Simul. **49**(5), 453–471 (2023).

[37] O. L. Anderson, "A simplified method for calculating the debye temperature from elastic constants," J. Phys. Chem. Solids **24**(7), 909–917 (1963).

[38] B. Weidenfeller, M. Höfer, and F. R. Schilling, "Thermal conductivity, thermal diffusivity, and specific heat capacity of particle filled polypropylene," Composites, Part A **35**(4), 423–429 (2004).

[39] G. Grimvall, *Thermophysical Properties of Materials* (Elsevier, 1999).

[40] O. Fursenko, J. Bauer, G. Lupina, P. Dudek, M. Lukosius, C. Wenger, and P. Zaumseil, "Optical properties and band gap characterization of high dielectric constant oxides," Thin Solid Films **520**(14), 4532–4535 (2012).

[41] H. R. Philipp and H. Ehrenreich, "Optical properties of semiconductors," Phys. Rev. **129**(4), 1550–1560 (1963).